Simultaneous Measurement of the Half-Life and Spectral Shape of ^{115}In β Decay with an Indium Iodide Cryogenic Calorimeter

L. Pagnanini,[1,2,3] G. Benato,[1,2] P. Carniti,[4,5] E. Celi,[1,2] D. Chiesa,[4,5] J. Corbett,[3] I. Dafinei,[1] S. Di Domizio,[6,7] P. Di Stefano,[3] S. Ghislandi,[1,2,*] C. Gotti,[5] D. L. Helis,[1,2,†] R. Knobel,[3] J. Kostensalo,[8] J. Kotila,[9,10,11,12] S. Nagorny,[3,13] G. Pessina,[5] S. Pirro,[2] S. Pozzi,[5] A. Puiu,[2] S. Quitadamo,[1,2] M. Sisti,[5] J. Suhonen,[9,12] and S. Kuznetsov[14]

[1]*Gran Sasso Science Institute, 67100 L'Aquila, Italy*
[2]*INFN - Laboratori Nazionali del Gran Sasso, I-67100 Assergi (AQ), Italy*
[3]*Department of Physics, Engineering Physics and Astronomy, Queen's University Kingston, Ontario, K7L 3N6 Kingston, Canada*
[4]*Dipartimento di Fisica, Università di Milano - Bicocca, I-20126 Milano, Italy*
[5]*INFN - Sezione di Milano - Bicocca, I-20126 Milano, Italy*
[6]*Dipartimento di Fisica, Università di Genova, I-16146 Genova, Italy*
[7]*INFN - Sezione di Genova, I-16146 Genova, Italy*
[8]*Natural Resources Institute Finland, Yliopistokatu 6B, FI-80100 Joensuu, Finland*
[9]*University of Jyväskylä, Department of Physics, P. O. Box 35 (YFL), FI-40014, Finland*
[10]*Finnish Institute for Educational Research, University of Jyväskylä, P.O. Box 35, FI-40014, Finland*
[11]*Center for Theoretical Physics, Sloane Physics Laboratory, Yale University, New Haven, Connecticut 06520-8120, USA*
[12]*International Centre for Advanced Training and Research in Physics (CIFRA), 077125 Bucharest-Magurele, Romania*
[13]*Arthur B. McDonald Canadian Astroparticle Physics Research Institute, Kingston, ON, K7L 3N6, Canada*
[14]*Prokhorov General Physics Institute of the Russian Academy of Sciences 119991, Moscow, 38 Vavilov str., Russia*

(Received 29 January 2024; revised 4 April 2024; accepted 14 June 2024; published 16 September 2024)

Current bounds on the neutrino Majorana mass are affected by significant uncertainties in the nuclear calculations for neutrinoless double-beta decay. A key issue for a data-driven improvement of the nuclear theory is the actual value of the axial coupling constant g_A, which can be investigated through forbidden β decays. We present the first measurement of the 4th-forbidden β decay of ^{115}In with a cryogenic calorimeter based on indium iodide. Exploiting the enhanced spectrum-shape method for the first time to this isotope, our study accurately determines simultaneously spectral shape, g_A, and half-life. The interacting shell model, which best fits our data, indicates a half-life for this decay at $T_{1/2} = (5.26 \pm 0.06) \times 10^{14}$ yr.

DOI: 10.1103/PhysRevLett.133.122501

Introduction—The search for neutrinoless double-beta decay ($0\nu\beta\beta$) is a crucial part of our quest to understand the deepest mysteries of the Universe [1]. The observation of this phenomenon would require a paradigm shift from the standard model of elementary particles and would reshape our understanding of the fundamental building blocks of matter. $0\nu\beta\beta$ is an extremely rare process where two neutrons (protons) in the nucleus are simultaneously transformed into protons (neutrons), with the emission of just two electrons (positrons) in the final state. If we observe this process, it would indicate that neutrinos are Majorana particles, which means they are their own antiparticles. The half-life of this process ($T^{0\nu}_{1/2}$) could provide insights into the absolute mass scale of neutrinos, which is still an unsolved issue in particle physics. Moreover, $0\nu\beta\beta$ is a lepton-number-violating transition, and its observation would support exciting theoretical frameworks in which leptons played a crucial role in creating the matter or antimatter asymmetry in the Universe [2,3]. The next-generation experiments in this field are designed to approach half-lives of the order of 10^{27}–10^{28} yr. The current most stringent limit is set on ^{136}Xe by KamLAND-Zen at 2.3×10^{26} yr (90% C.L.) [4]. This limit can be converted into a constraint on the effective Majorana mass ($m_{\beta\beta}$), which is the new-physics parameter governing $0\nu\beta\beta$, by using the formula

$$m_{\beta\beta} = \frac{m_e}{g_A^2 \cdot \mathcal{M}_{0\nu} \cdot \sqrt{T^{0\nu}_{1/2} \cdot G_{0\nu}}}, \tag{1}$$

where m_e is the electron mass, $G_{0\nu}$ the phase space factor, $\mathcal{M}_{0\nu}$ the nuclear matrix element (NME), and g_A the axial coupling constant. While $G_{0\nu}$ can be precisely calculated for each isotope [5,6], nuclear calculations of $\mathcal{M}_{0\nu}$ are

*Contact author: stefano.ghislandi@gssi.it
†Contact author: dounia.helis@lngs.infn.it

affected by large uncertainty and depend on whether or not the free-nucleon value of $g_A^{\text{free}} = 1.276\,41$ [7] measured in the neutron decay holds also in nuclear decays [1]. For these reasons, a single limit on $T_{1/2}^{0\nu}$ results in a range of limits for $m_{\beta\beta}$ determined by the largest and smallest NMEs, e.g., $m_{\beta\beta} < 36$–156 meV in the KamLAND-Zen analysis [4]. This uncertainty not only limits the conversion of the half-life into $m_{\beta\beta}$ in case of discovery, but also severely affects the isotope selection for next-to-next generation experiments. It is well known that isotopes with lower Q values ($Q_{\beta\beta}$) are disfavored by lower $G_{0\nu} \propto Q_{\beta\beta}^5$ and larger background [1], but this precious information could be misleading if the NME landscape is unclear. Therefore, a data-driven improvement of nuclear models is essential to ensure that theoretical and experimental efforts in the $0\nu\beta\beta$ sector are not nullified [8].

Data and physical processes that could help clarify the puzzle include single and double-charge exchange reactions [9–13], ordinary muon captures [14,15], two neutrino double beta decays [16,17], and forbidden nonunique β decays [18]. In particular, the latter are very interesting to investigate the origins of the quenching of g_A, being the shape of the forbidden nonunique β-decay spectrum highly dependent on the ratio of g_A/g_V [19]. Here $g_V = 1$ is the weak vector coupling, whose value is set by the conserved vector current (CVC) hypothesis [20]. This dependence is enabled by the subtle balance between the vector and the axial-vector parts of the β-decay spectral shape function [18]. In this context, several isotopes have been studied such as ^{113}Cd [21–23], ^{99}Tc [24], and ^{115}In [25] using the so-called spectrum-shape method (SSM) [26]. This theoretical framework matches with high precision the spectral shape of experimental data. However, the simultaneous prediction of the decay half-life is often far from being compatible with the measured values. Improvements of the models in this direction have been done during the last years within the so-called enhanced SSM theory [27–29], where the small relativistic NME (sNME) enters as an additional parameter, facilitating the adjustment of both partial half-life and spectral shape.

In this Letter, we present the first application of the enhanced SSM on ^{115}In. The measurement has been performed with a cryogenic calorimeter based on indium iodide (InI) crystal in the framework of the ACCESS project [30,31].

β decay and sNME—In the enhanced SSM, the sNME enters as a free parameter of the model, together with g_A, in order to fit the experimental β-decay spectral shape and half-life simultaneously. In the nuclear-structure calculations, the sNME includes contributions outside the nucleon major shell(s), where the proton and neutron Fermi surfaces lie. In particular, the sNME stems from the small component of the relativistic nucleon wave function. Moreover, in spite of its smallness, it can have a notable influence on the β-decay half-lives and electron spectral shapes through the related large phase-space factor. In an ideal case, namely, diagonalizing the full nuclear Hamiltonian for all nucleons within an infinite nuclear configurations Hilbert space, the value of the sNME is connected to the value of the so-called large vector NME (l-NME), by the CVC hypothesis [27]. In typical nuclear models, its value cannot be computed in a reliable way, therefore it is reasonable to determine the sNME through data. Additionally, the deviation between the measured sNME value and the CVC calculation quantifies the impact of model approximations. More details can be found in Refs. [32–34].

Detector setup and data analysis—Following the design principles outlined in Ref. [30], we conduct measurements on a $7 \times 7 \times 7$ mm^3 (InI) crystal. The crystal has a mass $m_{\text{InI}} = (1.91 \pm 0.01)$ g and it is equipped with a neutron transmutation doped (NTD) germanium thermistor ($3 \times 2 \times 0.5$ mm^3) to record particle interactions within its lattice. The detector rests on a copper holder connected to the mixing chamber of the CUPID R&D dilution refrigerator [35] installed in Hall A of the Laboratori Nazionali del Gran Sasso, Italy. The setup is cooled down to approximately 16 mK. During the whole data-taking process, we use a thoriated wire as a permanent ^{232}Th calibration source mounted close to the detector. Periodic calibrations with external sources would have been more difficult due to the small size of the crystal and the presence of a lead shield in the cryostat. We estimate the amplitude of the acquired thermal pulses by applying the optimum filter [36]. We then perform a stabilization of the detector thermal gain due to temperature drifts by using the 238.6 keV γ-ray line of ^{212}Pb within the decay chain of ^{232}Th in the source [37]. Consequently, we calibrate in energy the stabilized spectrum using the most prominent peaks visible in the data. We observe an energy resolution of 3.9 keV (FWHM) at 238.6 keV. The detection threshold, defined as 5 times the baseline root-mean square, is estimated to be 3.4 keV. The criteria for selecting the events are based on rejecting noisy acquisition time intervals and windows that have more than one triggered pulse, which is commonly known as a distinguishable pileup. Additionally, we apply pulse-shape cuts requiring a constant selection efficiency as a function of the energy. This is mandatory to avoid any possible distortion in the spectral shape due to analysis. The overall analysis cut efficiency is $\epsilon = (52.2 \pm 0.3)\%$, where the distinguishable pileup cut dominates.

Data modeling and spectral fit—The study of the ^{115}In β-decay shape and the estimation of its half-life can be achieved through a background decomposition of the collected data. For this purpose, the geometry of the experimental setup is implemented into a GEANT4-based [38] simulation. We included electromagnetic and hadronic processes by using the QGSP_BERT_HP physics list. In the following, we define as *signal* the β spectrum of the ^{115}In [$Q_\beta = 497.489(10)$ keV [39]], and as *background* all

the remaining contributions required to explain the energy spectrum measured by the InI crystal. For the signal, we generate electrons uniformly distributed in the crystal. Their energy spectrum is sampled from templates obtained within three different theoretical frameworks: Interacting Shell Model (ISM) [40], Microscopic Quasiparticle-Phonon Model (MQPM) [41], and Interacting Boson-Fermion model (IBFM-2) [42]. These templates are calculated for values of g_A and sNME, which vary in the range [0.60, 1.39] and $[-5.9, 5.9]$ and with steps of 0.01 and 0.1, respectively. If needed, we use linear spline interpolation to increase the template fine structure. The most prominent background comes from the thoriated wire used as a calibration source. In order to account for a possible breaking of the secular equilibrium, we separately simulate the partial decay chain from ^{232}Th to ^{228}Ac and the remaining one starting from ^{228}Th. Any other potential background contribution, whether from the crystal or the cryogenic setup [43], is smaller than the statistical uncertainty associated to the bin counts. The Monte Carlo simulations undergo a postprocessing step that takes into account the effects of unresolvable pileup and finite energy resolution. The fit is performed in the energy range of [80, 800] keV. At lower energies, the data reconstruction is not satisfactory, while at higher energies the statistics is scarce. A uniform binning of 10 keV is chosen to avoid systematic effects due to the peak line shape.

We assume that the number of observed counts n_i in the ith bin follows the Poisson probability distribution:

$$P(n_i|\nu_i) = \frac{\nu_i^{n_i} \cdot e^{-\nu_i}}{n_i!}, \tag{2}$$

where ν_i is the number of expected events in the same bin. ν consists of a linear combination of the signal template $S(g_A, \text{sNME})$ and background simulations B_j, where $j = 1, 2$ identifies the ^{232}Th and ^{228}Th contributions from the calibration source. We introduce the normalization factors N_S and $N_{B,j}$, proportional to the half-life of ^{115}In ($T_{1/2}$) and to the activities of the background components, respectively. The expected number of events for each bin can be expressed as

$$\nu_i = N_S(T_{1/2}) \cdot S(g_A, \text{sNME})_i + \sum_{j=1,2} N_{B,j} \cdot (B_j)_i. \tag{3}$$

The likelihood can be therefore written as

$$\mathcal{L}(\text{data}|T_{1/2}, g_A, \text{sNME}, N_{B,j}) = \prod_i P(n_i, \nu_i). \tag{4}$$

The fit includes five free parameters: three are continuous ($T_{1/2}$ and $N_{B,j}$ with $j = 1, 2$), while the remaining two are discrete, namely, g_A and sNME. The two latter parameters identify the theoretical template to be picked at every step of the Markov-chain Monte Carlo used for the posterior sampling. We assume uniform prior probability distributions for all these parameters. Additionally, as a nuisance parameter, we introduce the analysis cut efficiency ϵ with a Gaussian prior probability distribution, in order to include its uncertainty and the correlations induced on the other fit parameters.

The ^{115}In half-life can be expressed as

$$T_{1/2} = \frac{\ln(2) \cdot t \cdot m_{InI} \cdot N_A \cdot \mathcal{IA}}{M_{InI} \cdot N_{decays}}, \tag{5}$$

where $t = 128.8$ h is the measurement time, N_A the Avogadro constant, $\mathcal{IA} = (95.719 \pm 0.052)\%$ [44] the natural isotopic abundance of ^{115}In, $M_{InI} = 241.72$ g/mol the molar mass of InI, and N_{decays} the total number of ^{115}In decays during t. The explicit dependence of N_{decays} on the other parameters is $N_{decays} = [(N_S \cdot N_{MC})/\epsilon]$, where N_{MC} corresponds to the total number of simulated ^{115}In β decays building $S(g_A, \text{sNME})$.

We use the Bayesian analysis toolkit (BAT) [45] to perform the statistical inference as well as the posterior sampling and marginalization. For each fit, we quote the median of the marginalized posterior as an estimator of the best value of the parameter at issue. The interval defined by [16, 84]% quantiles is used to evaluate the uncertainty. From this analysis, we also extract an experimental spectrum of ^{115}In β decay suitable for nuclear model comparison [33,46].

Analysis results—We perform the data reconstruction by using two different fit methods. The first is the *best fit*, which determines the configuration that best matches the

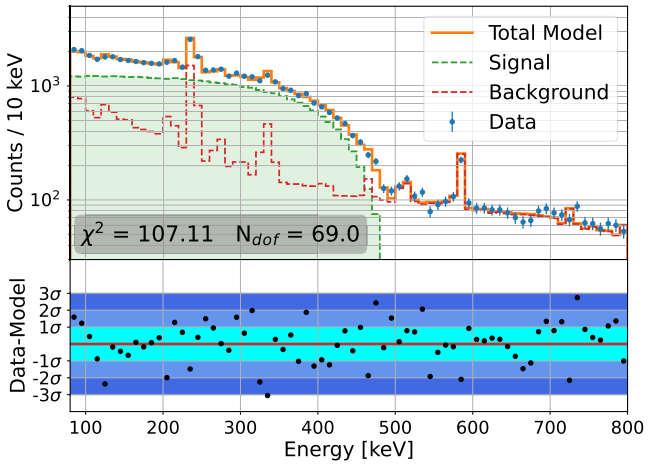

FIG. 1. Top: Experimental spectrum (blue dots) and best fit result (orange solid line) obtained within the interacting shell model, which results to be the most suitable to describe the data. The fit model is a linear combination of the ^{115}In β-decay template spectrum (green dashed line), and the contributions from the thorium calibration source (red dashed line). The χ^2 and the number of degrees of freedom N$_{dof}$ are reported. Bottom: Fit residuals normalized to the statistical uncertainty.

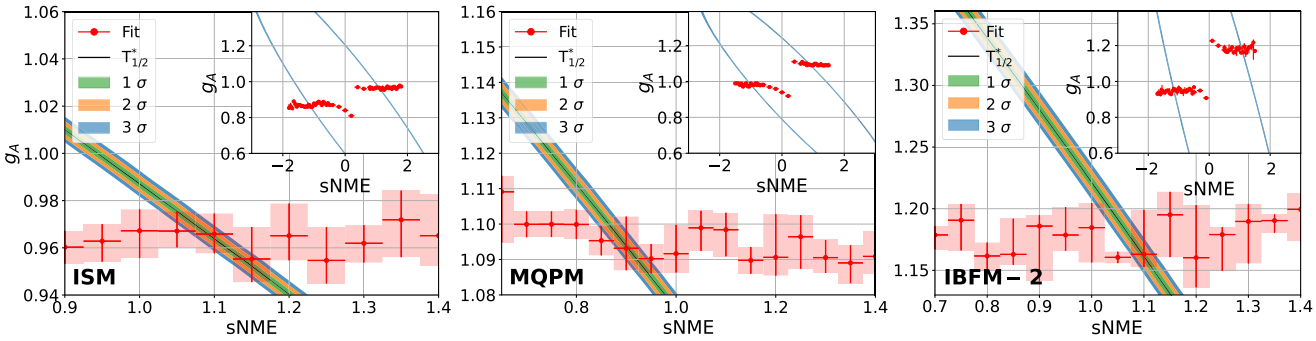

FIG. 2. Identification of the optimal sNME values with the *matched half-life fit* for ISM (left), MQPM (center), and IBFM-2 (right), respectively. The main plot reports as colored bands the half-life $T^*_{1/2}$ together with its uncertainties, and as red points the value of g_A that best fit the data for a fixed value of sNME. The uncertainty on the latter is fixed by the template fine structure, while the one on g_A is the [16, 84]% quantile interval from the Bayesian fit. Each inset shows the half-life dependence on the other two parameters of the theory, together with the fit results, in a wider sNME interval.

data by letting both g_A and sNME vary. Figure 1 depicts the data reconstruction through the best fit method achieved by using the ISM model. The second method, referred to as *matched half-life fit*, tests the core of the sNME approach, namely, the joint prediction of spectral shape and half-life. We vary the value of g_A while fixing sNME, treating it as a free parameter of the model. We then select the sNME by comparing the fit result with the known half-life $T^*_{1/2}$ in the (g_A, sNME) parameter space, where the trend of $T^*_{1/2}$ is predicted by the nuclear model being studied. The value of $T^*_{1/2}$ has been obtained as an average of previous measurements [25,47–49], weighted for their uncertainties, and is $T^*_{1/2} = (5.14 \pm 0.06) \times 10^{14}$ yr. This method is illustrated in Fig. 2 for the three nuclear models.

The results for the two fit techniques in the three theoretical frameworks are summarized in Table I, where the positive sNME solutions are reported. Negative solutions are disfavoured based on the reduced chi-square χ^2_{red}, and the resulting half-life is not compatible with $T^*_{1/2}$ [33]. Therefore, our discussion will focus on the positive sNME solutions.

TABLE I. Results for the two fit methods and the three considered nuclear models on the parameters of interest g_A, sNME, and $T_{1/2}$. The reduced chi-square χ^2_{red} is also reported as an estimator of the goodness of fit.

Model	g_A	sNME [fm^3]	$T_{1/2}/10^{14}$	χ^2_{red}
Best fit				
ISM	$0.964^{+0.010}_{-0.006}$	$1.75^{+0.13}_{-0.08}$	5.26 ± 0.06	1.55
MQPM	$1.104^{+0.019}_{-0.017}$	$2.88^{+0.49}_{-0.71}$	5.26 ± 0.07	1.65
IBFM-2	$1.172^{+0.022}_{-0.017}$	$0.81^{+0.52}_{-0.24}$	5.25 ± 0.07	1.66
Matched				
ISM	$0.965^{+0.013}_{-0.010}$	1.10 ± 0.03	5.20 ± 0.07	1.78
MQPM	$1.093^{+0.009}_{-0.007}$	0.90 ± 0.03	5.05 ± 0.06	2.32
IBFM-2	$1.163^{+0.036}_{-0.010}$	1.10 ± 0.03	5.28 ± 0.06	1.67

Considering the best fit method, we study the systematic effects due to the fit assumptions. The half-life values exhibit perfect agreement when changing the nuclear model. Conversely, g_A and sNME are strictly related to the approximations done within a specific theoretical framework, therefore we do not expect them to coincide for different models. Moreover, we reiterate the best fit by assuming secular equilibrium in ^{232}Th decay chain contained in the calibration source. We also study the binning effect by changing the bin width to 20 keV and varying both the upper energy limit to 550 and 1000 keV and the lower energy threshold to 150 keV. We do not include a test with an energy threshold below 80 keV since we cannot have a satisfactory reconstruction of the background below this energy. All the tested fit assumptions result in values for g_A, sNME, and half-life that are fully compatible within 1σ

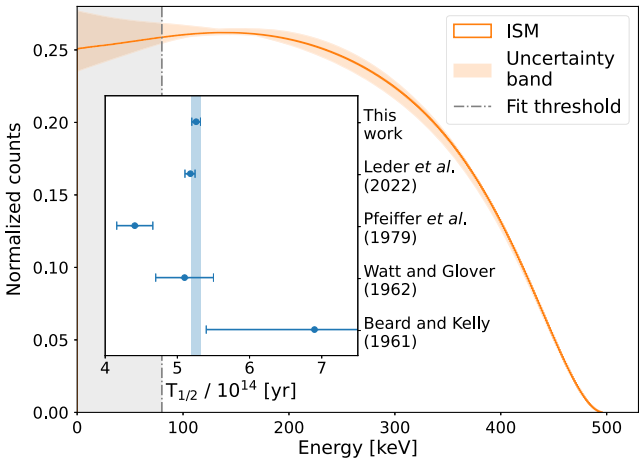

FIG. 3. Theoretical energy spectrum of ^{115}In β decay. The orange solid line corresponds to the best model fit (ISM) of the experimental data taken above 80 keV. The shaded band includes the variation of the three models considered within the 68% uncertainty interval for g_A and sNME. In the inset, we compare the half-life obtained here and in past works.

with the ones reported in Table I. In light of this, we pick as an overall half-life the one coming from the best fit of the ISM model, which shows the highest goodness of fit. We report in Fig. 3 the theoretical spectral shape of ^{115}In β decay obtained from the ISM best fit. We also show the uncertainty band obtained by varying g_A and sNME within the 1σ contour of the joint posterior for the three models.

Discussion—The ^{115}In β-decay measurement here presented improves the accuracy level of the most recent analysis in Ref. [25]. Indeed, different models reproduce as best fit the same half-life with compatible spectral shapes [33]. Moreover, this study has improved the energy threshold by a factor of two compared to Ref. [25]. This is a crucial step to reduce the model dependency of the results, since at energies $\lesssim$100 keV different models predict different spectral shapes. As pointed out in Ref. [50], a lower threshold is essential to reduce the impact of low-energy spectral shape extrapolations and make the half-life determination more reliable, especially when an additional free parameter is present. This measurement also confirms a noteworthy discrepancy with the spectral shape reported in Ref. [47], which could be affected by important systematic uncertainties due to the background subtractions.

Considering the best fit method, we consistently achieve a robust data reconstruction, obtaining a χ^2_{red} in the range [1.55, 1.66]. The signal-to-background ratio of the collected data limits the possibility of precisely determining g_A and sNME simultaneously within a single nuclear model. The sNME has a weaker impact on the spectral shape, therefore it is affected by a relatively high uncertainty, sometimes larger than 20%. We observe a clear preference for positive sNME solutions, aligning with the CVC predictions (i.e., 6.01 fm^3 for ISM, 10.25 fm^3 for MQPM, and 2.53 fm^3 for IBFM-2). In particular, the experimental values are consistently about one-third of the CVC ones indicating that the presently used models are not perfect many-body frameworks for ^{115}In as required by the exact CVC relation. The strong bias for the positive values of the sNME significantly helps in selecting the correct spectral shape when it strongly depends on sNME value, as in some cases discovered in the β-decay shape survey in Ref. [34].

For the three models, we obtain different values of g_A, still, they all strongly reject the free-nucleon hypothesis with a significance of at least 4.7σ. We can determine the half-life of the ^{115}In β decay with an accuracy of $\mathcal{O}(1\%)$ and all the obtained half-lives are fully compatible with each other. Furthermore, these values are in agreement with $T^*_{1/2}$ within 1.4σ, regardless of the theoretical model. However, the half-lives predicted by the models for the best fit parameters are 2.37×10^{14} yr (ISM), 8.52×10^{13} yr (MQPM), and 7.93×10^{14} yr (IBFM-2), far from the ones obtained with the fit.

It is therefore interesting to compare the best fit outcomes with those of the matched half-life fit, investigating how the matching of the predicted half-life impacts the results. In the cases of ISM and IBFM-2, the fit quality mildly worsens and the physical parameters g_A and $T_{1/2}$ are compatible, affirming the reliability and robustness of this method. By construction, the theoretical predictions on the half-lives agree with $T^*_{1/2}$ and are compatible within 1σ with the measured half-life. Conversely, the matched fit approach for the MQPM makes the model unable to describe the spectral shape. Moreover, the resulting half-life in this case is not compatible within 2σ with both theoretical predictions and all the other half-life determinations. This makes the joint prediction of spectral shape and half-life less reliable for this method.

The value of g_A reported for ^{115}In in Ref. [25] are significantly smaller than the ones obtained in the current work. It seems that usage of the sNME degree of freedom not only improves the agreement between experimental and theoretical values of the half-life, but also shifts g_A to bigger values. The same happens in ^{113}Cd for MQPM when going from the analysis in Ref. [22] to the one in Ref. [23], while for ISM and IBFM-2 the two results remain compatible. The analysis based on the spectral moments method in Ref. [51] applies a technique somehow similar to the matched half-life fit of this work. Even if applied on ^{113}Cd data, the results quoted in terms of g_A are very close to this work. These findings deserve careful examination and further insights in future nuclear-model computations. It is crucial that such calculations include predictions of β-decay spectral shapes based on the preferred values of the sNME within the enhanced SSM framework. In conclusion, the present study, as also those in Refs. [23,51], point to a moderate quenching of g_A in the highly forbidden β transitions. This, in turn, would suggest that both the allowed and forbidden virtual transitions in the $0\nu\beta\beta$ decay are quenched in a similar fashion and no separate quenching is needed for each multipole, making the evaluation of the $0\nu\beta\beta$ NMEs much easier. This hypothesis could work at least for $0\nu\beta\beta$ nuclei close to the mass region $A = 113$–115, i.e., for the $0\nu\beta\beta$ NMEs of ^{110}Pd, ^{112}Sn, ^{114}Cd, and ^{116}Cd. However, further β-spectral studies in other mass regions and for transitions of various forbiddenness should be carried out in order to validate the above hypothesis.

Acknowledgments—We thank Eligio Lisi, Antonio Marrone, Giovanni De Gregorio, Riccardo Mancino, Luigi Coraggio, and Nunzio Itaco for useful comments and discussions, which allowed us to present the results of this work more clearly. This project has received funding from the European Union's Horizon 2020 research and innovation program under the Marie Skłodowska-Curie Grant Agreement No. 101029688 (ACCESS—Array of Cryogenic Calorimeters to Evaluate Spectral Shape). This

work was supported by the Academy of Finland, Grants No. 314733, No. 320062, and No. 345869. J. Kotila and J. Suhonen acknowledge support from project PNRR-I8/C9-CF264, Contract No. 760100/23.05.2023 of the Romanian Ministry of Research, Innovation, and Digitization (the NEPTUN project). We thank the CUPID Collaboration for sharing their cryogenic infrastructure, M. Guetti for the assistance in the cryogenic operations, M. Perego for his invaluable help in many tasks, the mechanical workshop of LNGS.

[1] M. Agostini, G. Benato, J. A. Detwiler, J. Menéndez, and F. Vissani, Rev. Mod. Phys. **95**, 025002 (2023).
[2] W. Buchmüller, R. D. Peccei, and T. Yanagida, Annu. Rev. Nucl. Part. Sci. **55**, 311 (2005).
[3] L. Canetti, M. Drewes, and M. Shaposhnikov, New J. Phys. **14**, 095012 (2012).
[4] S. Abe *et al.* (KamLAND-Zen Collaboration), Phys. Rev. Lett. **130**, 051801 (2023).
[5] J. Kotila and F. Iachello, Phys. Rev. C **85**, 034316 (2012).
[6] S. Stoica and M. Mirea, Front. Phys. **7**, 12 (2019).
[7] B. Märkisch *et al.*, Phys. Rev. Lett. **122**, 242501 (2019).
[8] P. Gysbers *et al.*, Nat. Phys. **15**, 428 (2019).
[9] D. Frekers and M. Alanssari, Eur. Phys. J. A **54**, 177 (2018).
[10] P. Puppe, A. Lennarz, T. Adachi, H. Akimune, H. Ejiri *et al.*, Phys. Rev. C **86**, 044603 (2012).
[11] F. Cappuzzello *et al.* (NUMEN Collaboration), Prog. Part. Nucl. Phys. **128**, 103999 (2023).
[12] H. Lenske, J. I. Bellone, M. Colonna, and J.-A. Lay, Phys. Rev. C **98**, 044620 (2018).
[13] H. Ejiri, Universe **8**, 457 (2022).
[14] I. H. Hashim *et al.*, Phys. Rev. C **108**, 014618 (2023).
[15] P. Gimeno, L. Jokiniemi, J. Kotila, M. Ramalho, and J. Suhonen, Universe **9**, 270 (2023).
[16] J. Barea, J. Kotila, and F. Iachello, Phys. Rev. C **87**, 014315 (2013).
[17] C. Augier *et al.* (CUPID-Mo Collaboration), Phys. Rev. Lett. **131**, 162501 (2023).
[18] H. Ejiri, J. Suhonen, and K. Zuber, Phys. Rep. **797**, 1 (2019).
[19] M. Haaranen, J. Kotila, and J. Suhonen, Phys. Rev. C **95**, 024327 (2017).
[20] R. P. Feynman and M. Gell-Mann, Phys. Rev. **109**, 193 (1958).
[21] P. Belli, R. Bernabei, N. Bukilic, F. Cappella, R. Cerulli *et al.*, Phys. Rev. C **76**, 064603 (2007).
[22] L. Bodenstein-Dresler and *et al.* (COBRA Collaboration), Phys. Lett. B **800**, 135092 (2020).
[23] J. Kostensalo, J. Suhonen, J. Volkmer, S. Zatschler, and K. Zuber, Phys. Lett. B **822**, 136652 (2021).
[24] M. Paulsen *et al.*, arXiv:2309.14014.
[25] A. F. Leder, D. Mayer, J. L. Ouellet, F. A. Danevich, L. Dumoulin *et al.*, Phys. Rev. Lett. **129**, 232502 (2022).
[26] M. Haaranen, P. C. Srivastava, and J. Suhonen, Phys. Rev. C **93**, 034308 (2016).
[27] H. Behrens and W. Bühring, *Electron Radial Wave Functions and Nuclear Beta-Decay* (Clarendon Press, Oxford, 1982).
[28] A. Kumar, P. C. Srivastava, J. Kostensalo, and J. Suhonen, Phys. Rev. C **101**, 064304 (2020).
[29] A. Kumar, P. C. Srivastava, and J. Suhonen, Eur. Phys. J. A **57**, 225 (2021).
[30] L. Pagnanini *et al.* (ACCESS Collaboration), Eur. Phys. J. Plus **138**, 445 (2023).
[31] E. Celi, Z. Galazka, M. Laubenstein, S. Nagorny, L. Pagnanini, S. Pirro, and A. Puiu, Nucl. Instrum. Methods Phys. Res., Sect. A **1033**, 166682 (2022).
[32] J. Suhonen, *From Nucleons to Nucleus* (Springer, New York, 2007).
[33] See Supplemental Material at http://link.aps.org/supplemental/10.1103/PhysRevLett.133.122501 for further details. Supplemental Material consists of two sections. The first offers a theoretical summary of the small nuclear matrix element approach and discusses various nuclear models. The second section provides additional details about the data acquisition system, the analysis chain and the interpretation of the results, with a focus on the low energy region below the threshold. It also includes the complete fit results with negative small nuclear matrix elements.
[34] M. Ramalho and J. Suhonen, Phys. Rev. C **109**, 034321 (2024).
[35] O. Azzolini *et al.* (CUPID Collaboration), Eur. Phys. J. C **78**, 428 (2018).
[36] E. Gatti and P. F. Manfredi, Riv. Nuovo Cimento **9**, 1 (1986).
[37] C. Alduino *et al.* (CUORE Collaboration), Phys. Rev. C **93**, 045503 (2016).
[38] S. Agostinelli *et al.* (GEANT4 Collaboration), Nucl. Instrum. Methods Phys. Res., Sect. A **506**, 250 (2003).
[39] J. Blachot, Nucl. Data Sheets **113**, 2391 (2012).
[40] E. Caurier, G. Martinez-Pinedo, F. Nowack, A. Poves, and A. P. Zuker, Rev. Mod. Phys. **77**, 427 (2005).
[41] J. Toivanen and J. Suhonen, Phys. Rev. C **57**, 1237 (1998).
[42] F. Iachello and P. v. Isacker, *The Interacting Boson-Fermion Model*, Cambridge Monographs on Mathematical Physics (Cambridge University Press, Cambridge, England, 1991).
[43] O. Azzolini *et al.* (CUPID-0 Collaboration), Phys. Rev. Lett. **131**, 222501 (2023).
[44] J. R. de Laeter, J. K. Böhlke, P. D. Bièvre, H. Hidaka, H. S. Peiser, K. J. R. Rosman, and P. D. P. Taylor, Pure Appl. Chem. **75**, 683 (2003).
[45] O. Schulz, F. Beaujean, A. Caldwell, C. Grunwald, V. Hafych, K. Kröninger, S. La Cagnina, L. Röhrig, and L. Shtembari, SN Comput. Sci. **2**, 1 (2021).
[46] G. De Gregorio, R. Mancino, L. Coraggio, and N. Itaco, Phys. Rev. C **110**, 014324 (2024).
[47] L. Pfeiffer, A. P. Mills, E. A. Chandross, and T. Kovacs, Phys. Rev. C **19**, 1035 (1979).
[48] D. E. Watt and R. N. Glover, Philos. Mag. **7**, 105 (1962).
[49] G. B. Beard and W. H. Kelly, Phys. Rev. **122**, 1576 (1961).
[50] J. Kostensalo, E. Lisi, A. Marrone, and J. Suhonen, arXiv:2405.11920.
[51] J. Kostensalo, E. Lisi, A. Marrone, and J. Suhonen, Phys. Rev. C **107**, 055502 (2023).